Published on J Comp Neurol on Sept. 30, 2019; https://doi.org/10.1002/cne.24776

Lumbar spinal cord neurons putatively involved in ejaculation are sexually dimorphic in early postnatal mice

Running title: Sexual dimorphism in LSt neurons

Giuseppe Federighi[1] | Sabrina Asteriti[2] | Lorenzo Cangiano[1]

[1]Dept. of Translational Research, University of Pisa, Pisa, Italy

[2]Dept. of Neurosciences, Biomedicine and Movement Sciences, University of Verona, Verona, Italy

Correspondence: Prof. Lorenzo Cangiano, Istituto di Fisiologia, Via San Zeno 31, 56123 Pisa, Italy, lorenzo.cangiano@unipi.it

Acknowledgements

We thank Mr. Arsenio Armagno and Dr. Marcello Raspa at the Consiglio Nazionale delle Ricerche, European Mouse Mutant Archive (EMMA) – Monterotondo Campus International Development INFRAFRONTIER I3, "A. Buzzati-Traverso" Campus, Monterotondo Scalo (Roma, Italy) for excellent assistance with import and resuscitation of the Gal-eGFP mouse line, and Dr. Rossana Scuri at the University of Pisa for kind access to sequencing resources. Funding was provided by the University of Pisa as intramural grants.

Data Availability Statement: The data that support the findings of this study and all custom scripts are available from the corresponding author upon reasonable request.

ABSTRACT

A crucial role in ejaculation is thought to be played by a population of lumbar spino-thalamic neurons (LSt), which express galanin and other neuropeptides. In rats, these neurons are activated with ejaculation and their lesion selectively abolishes ejaculation but not other mating behaviors. Consistently with their role, in adult rats and humans, LSt neurons are sexually dimorphic, being more numerous in males.

Here we examined whether sexual dimorphism arises early in development, using a transgenic mouse line in which the expression of fluorescent protein is driven by the galanin promoter. We focused on postnatal day 4, shortly after a transient perinatal androgen surge in males that could play an organizational role in LSt development.

We found a population of brightly fluorescent neurons organized in bilateral columns dorsolateral to the central canal in segments L1–L5, the expected location of the LSt group. Their number was close to that of adult preparations and significantly greater in male than in female siblings (+19%; $CI_{95\%}$: +13% to +27%; $p<0.01$). This was not due to a generalized higher galanin expression in the male since fluorescent L4 DRG neurons, innervating the hindlimbs and lower back, were not significantly dimorphic (–4%; $CI_{95\%}$: –10% to +8%; $p=0.92$). Unexpectedly, we found in cervical segments a population of fluorescent neurons having a location relative to the central canal similar to the LSt.

Thus, the LSt group is sexually dimorphic soon after birth. However, it is possible that only a subset of its neurons participate in the control of ejaculation.

Keywords: spinal cord, galanin, ejaculation, sexual dimorphism, neurons, mice, RRID:MMRRC_016342-UCD, RRID:SCR_016865, RRID:SCR_002285, RRID:SCR_015823.

1 | INTRODUCTION

The motor pattern of ejaculation consists of two sequential phases: emission of the components of semen into the urethral meatus via smooth muscle contraction of the prostate, seminal vesicles and *ductus deferens*, and expulsion from the urethra through rhythmic striated muscle contractions (Clement & Giuliano, 2016). At the level of the spinal cord the corresponding autonomic and somatic motoneurons are distributed from thoracolumbar to sacral segments. The expression of ejaculation and the coordination of the various motor nuclei are controlled by a dedicated premotor network, the *spinal generator of ejaculation* (SGE), largely localized in the lumbar enlargement. Evidence in support of this includes, in men, the capacity to ejaculate in patients with complete spinal sections above T12 but not when the lesion involved the lumbar cord (Chapelle et al., 1988; Chéhensse et al., 2016). Furthermore, in spinalized rats electrical micro-stimulation in a restricted volume around the central canal between L1 and L5 evokes the full ejaculatory pattern (Borgdorff et al., 2008).

A crucial role in this well defined region is played by a population of so-called lumbar spino-thalamic neurons (LSt), whose somas lie in laminae VII and X. These were originally identified as a well-defined population in rats by their co-expression of the peptides galanin and cholecystokinin (CCK) (Ju et al., 1987), but were later also found to express enkephalin (Nicholas et al., 1999), NK-1 receptor (Truitt & Coolen, 2002) and the gastrin releasing peptide (GRP) (Kozyrev et al., 2012; Sakamoto et al., 2008). There is clear evidence that at least some of these neurons project to the parvocellular subparafascicular thalamic nucleus (Coolen et al., 2003; Ju et al., 1997), hence their name. Within the LSt group, neurons were found having an increased c-fos expression specifically following ejaculation and not other components of male sexual behavior (Truitt et al., 2003). Furthermore, their selective ablation with the toxin saporin conjugated to a high affinity NK-1R agonist abolished ejaculation but not erection, mounts and intromissions in freely-behaving rats (Truitt & Coolen, 2002). Transsynaptic retrograde labelling from the prostate, bulbospongiosus muscle and seminal vesicles double labelled LSt neurons (Sun et al., 2009; Xu et al., 2006), suggesting that they have collateral projections to the pre-ganglionic neurons and somatic motoneurons involved in emission and expulsion. The effects of LSt neuron ablation described above were further extended to spinalized rats (Staudt et al., 2012), again supporting the existence of propriospinal connections and their role as pre-motor interneurons.

An additional characteristic of LSt neurons, consistent with their role in sexual function, is that in adults they are more numerous in adult males than females as assessed by galanin, CCK or GRP expression in rats (Newton, 1992b; Phan & Newton, 1999; Sakamoto et al., 2008) and galanin in humans (Chéhensse et al., 2016). Like the well-known sexual dimorphism of perineal motoneurons (Breedlove & Arnold, 1983), that of the LSt population is regulated by androgen receptors, since rats with the testicular feminization mutation (Tfm) displayed hyper-feminine numbers of LSt neurons (Newton & Phan, 2006; Sakamoto et al., 2008). Furthermore, delivery of androgen to newborn females led to male-like LSt neuron numbers in the adult, as assessed by GRP expression (Oti et al., 2016). Since male rodents undergo a transient testosterone surge at birth (Clarkson & Herbison, 2016), it is likely that this event plays an important organizational role (i.e. permanent; Forger, 2009) in the development of LSt neuron dimorphism.

Here we examined the LSt neuron population at postnatal day 4 (P4), much earlier than previous studies, to assess whether sexual dimorphism is established soon after the testosterone surge has ended. As a quantitative proxy for galanin expression (Garcia et al., 2011) we employed a transgenic mouse line, previously validated in the brain (Laque et al., 2013), in which expression of the enhanced green fluorescent protein (eGFP) is driven by the galanin promoter.

2 | MATERIALS AND METHODS

2.1 | Animals and dissection

Gal-eGFP$^{+/+}$ mice were generated from CD-1 host females fertilized with STOCK Tg(Gal-EGFP)HX109Gsat/Mmucd (RRID:MMRRC_016342-UCD) sperm from GENSAT (The GENSAT Project). The resulting heterozygous progeny were iteratively inbred for several generations, each time selecting those individuals with the highest amount of the transgene as estimated with qPCR (Tesson et al., 2002). The mice were kept on a 12-12 hrs light-dark cycle with free access to food and water. No morphological or behavioral abnormalities were apparent in Gal-eGFP$^{+/+}$ mice relative to their CD-1 background strain. On the day of the experiment early postnatal females and males in each litter were distinguished on the basis of anogenital distance (Schneider et al., 1978),

an approach that we validated in separate tests in which litters were followed to adulthood (not shown).

All procedures involving the handling of experimental animals were approved by the ethical committee of the University of Pisa (n. 10/2018 as per D.lgs.vo 26/2014) and were conducted in accordance with Italian and EU regulations.

Mice of age P4 were decapitated, eviscerated and the spinal cord exposed by ventral laminectomy in room temperature oxygenated ACSF containing (in mM): 109 NaCl, 25 Glucose, 10 Hepes-Na, 5 Ascorbate-Na, 3 Pyruvate-Na, 2 $MgSO_4$ heptahydrate, 2 $CaCl_2$, 2 Thiourea, 2 KCl, 1.25 KH_2PO_4, 1 $NaHCO_3$ (pH adjusted to 7.40 with HCl and osmolality to 290 mOsm/Kg H_2O). Depending on the type of experiment either the spinal cord or the L4 dorsal root ganglia (DRGs) were removed. This and subsequent tissue handling procedures were performed under red light to prevent eGFP photobleaching.

2.2 | Imaging

The imaging system consisted of a DM LFSA upright microscope (Leica Microsystems, Wetzlar, Germany) equipped with a 49020 narrow band EGFP filter set (Chroma, Bellows Falls VT, USA), 4x/0.1NA air or 10x/0.3NA water objectives (Leica) and a DFC 350FX cooled monochrome camera (Leica) coupled with a 0.63x tube. Image stacks were acquired with μManager microscopy software (micro-manager.org, RRID:SCR_016865) (Edelstein et al., 2010) at sampling intervals of 1.543x1.543x10 μm/voxel (4x obj) or 0.649x0.649x5 μm/voxel (10x obj), close to (in x-y) or below (in z) the Nyquist sampling interval. Before acquisition the Hg lamp was allowed to stabilize for >30 min.

2.2.1 | Live transverse spinal cord slices

The isolated spinal cord was laid dorsal side up on 0.8 μm black filter paper (AABP02500; Merck, Darmstadt, Germany) glued to a platform with silicone grease, embedded in a thin layer of 3.5% low gelling temperature agarose (A9414; Sigma-Aldrich/Merck) and covered with room temperature ACSF. Transverse spinal cord sections were made with a manual tissue chopper (Leica

Biosystems, Wetzlar, Germany) at 500 μm intervals using PTFE-coated razor blades. Multiple photos of the sectioned cord were taken through an ocular of the dissection microscope and combined with a super resolution algorithm (Northrup, 2018) in Photoshop (Adobe, San Jose CA, USA). Starting from the caudal end, each slice was visually (and later photographically) identified by its position relative to a reference grid drawn on the platform and transferred, caudal cut face up together with the supporting filter paper strip, to a large multi-well container flooded with ACSF. For each slice a volume of 2148x1605x610 μm centered on its upper (i.e. caudal) cut surface was imaged (4x obj; stack of 61 x 4000 ms exposures).

2.2.2 | Fixed and cleared spinal cord wholemounts

The isolated spinal cord was fixed in 4% paraformaldehyde in PBS (~1 hour at 4°C) and rinsed in PBS (4 x 10 min washes). It was then laid dorsal side up on filter paper glued with silicone grease to a small plastic disk, embedded in a thin layer of 3.5% agarose and covered with PBS. The disk+filter+cord block was fixed to the platform of a vibratome (VT 1200S; Leica Biosystems), submerged in ice-cold PBS and the dorsal-most 150–200 μm of the lumbar enlargement removed under stereo microscope inspection. The block was then transferred to a 35 mm Petri dish for processing with the tissue clearing FRUIT protocol (Hou et al., 2015): 45 min in 35% FRUIT, 35 min each in 40/60/80% FRUIT, >1 hr in 100% FRUIT (all with constant agitation at room temperature) and finally stored in 100% FRUIT at 4°C (all components of FRUIT from Sigma-Merck). For imaging the block was transferred to the middle of a large Petri dish and covered with 100% FRUIT just enough to have a perfectly flat air/liquid interface. Overlapping tiles of cord were acquired, each in an imaged volume of 2148x1605x1310 μm (4x obj; stack of 131 x 8000 ms exposures). In all these experiments pairs of female/male siblings from the same litter were processed in parallel.

2.2.3 | Fixed and cleared DRGs

The ganglia were fixed in 4% paraformaldehyde in PBS (~30 min at 4°C) and rinsed in PBS (4 x 10 min washes). They were then laid on filter paper glued with silicone grease to a small plastic disk, embedded in a very thin layer of 1% agarose and covered with PBS. The disk+filter+DRGs block

was then transferred to a 35 mm Petri dish for FRUIT tissue clearing. For imaging the dish was filled with 80% or 100% FRUIT into which the 10x water objective was dipped. A single tile centered on a DRG was acquired with a volume of 904x675x905 μm (10x obj; stack of 181 x 2000 ms exposures). DRGs from female and male siblings from the same litter were processed in parallel.

2.3 | Image stack pre-processing and deconvolution

Image analysis was performed with Fiji/ImageJ (fiji.sc, RRID:SCR_002285) (Schindelin et al., 2012; Rueden et al., 2017) using public domain plugins and custom scripts. All stacks were pre-processed as follows: (i) bit depth was extended to 32 bits; (ii) the average dark noise generated by the CCD was separately measured and subtracted; (iii) uneven illumination by the Hg lamp was separately measured and compensated; (iv) a small constant was added and negative pixels set to zero. For spinal cord slices and wholemounts (but not for DRGs, except in the preparation of Figure 4), the pre-processed stacks were deconvolved with the DeconvolutionLab2 plugin (bigwww.epfl.ch/deconvolution/deconvolutionlab2/) (Sage et al., 2017) (Richardson & Lucy, N = 100). An approximation of the point spread function (psf) of the optical system equipped with a 4x air objective was obtained with PSF Generator (bigwww.epfl.ch/algorithms/psfgenerator/) (Kirshner et al., 2013) (Richards & Wolfe, 510 nm, ni = 1.02, NA = 0.1). This theoretical psf was in line with (data not shown) an experimental psf obtained by averaging many green fluorescent beads embedded in agarose (1 μm, L4655; Sigma-Merck) using PSF Creator and PSF Combiner in the GDSC suite (www.sussex.ac.uk/gdsc/intranet/microscopy/UserSupport/AnalysisProtocol/imagej/smlm_plugins) by Alex Herbert (University of Sussex). The theoretical psf was thereafter employed for deconvolution because of its lack of noise.

2.3.1 | Live slice image processing

Deconvolved stacks were processed with the Extended Depth of Field plugin (bigwww.epfl.ch/demo/edf/) using complex wavelets (Forster et al., 2004), resulting in a single image of the in-focus surface of the slice. Each image was assigned to its spinal segment of origin by projecting the photo of the sectioned spinal cord (see 2.2.1) onto a reference map of segments drawn with the aid of

super-resolution photos of a spinal cord: the border between segments was taken at the midpoint between adjacent rootlet fans. For each animal 0, 1 or 2 slices fell in any given segment. Images at this stage of the processing pipeline are shown in Figure 1. Subsequently each image was duplicated and one of its two copies flipped so as to have both hemisegments represented on the right-hand side. All images in which the right hemisegment had debris on the cut surface or was markedly deformed by sectioning were discarded. On the remaining set of right hemisegments (384 images from C3 to Co1) the following point and freeline ROIs were manually annotated in the image overlay: central canal (point), contour of dorsal lamina I (freeline), lateral and ventral contours (fr.), lateral margin of the contralateral hemisegment (fr.). Thereafter, all images from the same spinal segment (or pair of adjacent segments in the case of the rostral cord) were registered to a template for that specific segment with the Landmark Correspondences plugin (imagej.net/Landmark_Correspondences) (Shaefer et al., 2006) in 'rigid transformation' mode. From these data we derived the brightness and hue channels of an HSB color model for the images shown in Figure 2, as described below. Brightness channel: for each segment (or segment pair) all registered images were Gaussian blurred (sigma = 7–14 px depending on sample and segment size), averaged together, log-transformed (to reduce the dynamic range and adequately represent both dim neuron-rich regions and the bright dorsal laminae) and linearly scaled to optimize contrast (the brightest pixel in each right hemisegment was at saturation). Hue channel: all registered images were processed with Trainable Weka Segmentation (imagej.net/Trainable_Weka_Segmentation) (Arganda-Carreras et al., 2017) using the same classifier (previously trained to identify bona fide neurons in a small sample of images from different segments). For each segment (or segment pair) all classified images were logically combined with an OR operation, Gaussian blurred (sigma = 3 times the value used for brightness), thresholded and linearly scaled between the values for yellow (no neurons) and red (neurons). Saturation channel: set at maximum. Finally, each right hemisegment was duplicated, a copy flipped horizontally and the two copies merged at the midline into a full segment image.

Note that in Figure 1 and Figure 2 we present the cervical and first thoracic segments in pairs (C3–C4, … , T5–T6). This approach was adopted due to the fact that rostral segments are shorter than caudal ones, with the goal of maintaining two parameters relatively constant along the length of the cord: (i) precision in segment identification, (ii) the number of slices per segment or segment pair.

2.3.2 | Fixed and cleared spinal cord wholemounts image processing

For each spinal cord all the individual overlapping tiles were merged into a single stack using the BigStitcher plugin (imagej.net/BigStitcher) (Hörl et al., 2018). This was in turn filtered with the LoG 3D plugin (bigwww.epfl.ch/sage/soft/LoG3D/) (Sage et al., 2005) to enhance ellipsoidal particles on the neuronal scale. Then, a 3D Gaussian-blurred copy of the same stack was subtracted to remove slow-varying background fluorescence. Finally, individual neurons were identified for counting with the FindFoci plugin (www.sussex.ac.uk/gdsc/intranet/microscopy/UserSupport/AnalysisProtocol/imagej/findfoci) (Herbert et al., 2014), after masking out extraneous volumes. Throughout this processing pipeline all parameters were rigorously maintained identical for cords from female and male siblings.

2.3.3 | Fixed and cleared DRGs image processing

Stacks were filtered with the LoG 3D plugin to enhance blob-like objects on the neuronal scale. A 3D Gaussian-blurred copy of the same stack was subtracted to remove slow-varying background fluorescence. Individual neurons were identified for counting with FindFoci. All parameters were maintained identical for DRGs from female and male siblings.

2.4 | Statistical analysis

Statistics were computed with JASP 0.9.2 (jasp-stats.org, RRID:SCR_015823) (JASP Team 2019). Data are reported as median and interquartile range (with median included in quartile calculation) or Hodges-Lehmann estimator of the center of a distribution and its 95% confidence interval ($CI_{95\%}$) (Hershberger, 2011). The non parametric tests used were: paired directional Wilcoxon signed-rank (pdW) test, independent directional Mann-Whitney (idMW) test.

3 | RESULTS

3.1 | General distribution of galanin reporter expression

We first assessed the distribution and expression level of the galanin reporter protein eGFP at postnatal day 4 (P4), by visualizing live transverse spinal cord slices from Gal-eGFP$^{+/+}$ mice with an upright epifluorescence microscope equipped with a low magnification 4x air objective. Figure 1 shows representative examples from cervical to coccygeal segments. Brightly fluorescent fibers and neurons were present throughout the spinal cord in what appeared to be well defined locations. However, to obtain a reliable assessment of the distribution of fluorescent neurons and avoid potentially misleading conclusions based on single slices, we performed a quantitative analysis combining, for each segment, data from several animals. Briefly (full details in 2.3.1) slices from the same segment were registered to each other and processed with a machine learning algorithm trained to identify neuronal somas, averaged and color-coded with *brightness* representing fluorescent intensity on a log scale and *hue* representing the relative likelihood of cell bodies being the source of such brightness. Figure 2 presents the final output of this processing pipeline, with each image combining data from 8 to 26 hemisegment images (median = 15, total = 384; 5 males and 4 females).

A dense mesh of fluorescent fibers was present in the dorsal-most cord of the Gal-eGFP$^{+/+}$ line at P4 in all examined spinal segments. At least part of these fibers belonged to primary afferents, since dorsal roots and dorsal root ganglia (DRGs) were brightly fluorescent (Figure 1 C5-C6,L3,L4; Figure 3; Figure 4). Often it was possible to distinguish fluorescence in the dorsal cord, having a thin laminar distribution, from that in an overlying dorsal rootlet (Figure 1 L4,L5,S3). A dorsal view of the entire spinal cord revealed diffuse fluorescence with a superficial web-like network of brighter threads (Figure 5).

A prominent feature of this mouse line was a population of brightly fluorescent neurons in segments L1–L5, tapering out rostrally in T12–T13 and caudally in L6. They were organized in two parallel columns located dorsolaterally in relation to the central canal (Figure 1; Figure 2, arrows), which shifted ventrally and expanded laterally when moving in the rostrocaudal direction. The spatial

distribution of this population matched what had been previously reported for the galaninergic LSt neurons thought to participate in the control of ejaculation.

Unexpectedly (see 4.2), a population of neurons in the cervical enlargement had a similar location to the lumbar LSt group, i.e. dorsal and lateral to the central canal (Figure 1 and Figure 2, C3–T4, arrows). Careful examination of intervening segments (Figure 2, T5–T11) revealed a sparse but uninterrupted presence of galaninergic neurons dorsolateral of the central canal, suggesting that the cervical, thoracic and lumbar populations may form a continuum.

Also of note was the presence, throughout the cord, of bright cell bodies in ventral laminae compatible with their being motoneurons. Consistent with this interpretation, we found that the ventral roots were fluorescent (Figure 1 L1–L4, S3), albeit much less so than dorsal roots (Figure 3).

Lastly, in sacral and coccygeal segments a compact lateral population of neurons was present (Figure 1 and Figure 2, S1–Co1).

3.2 | Galaninergic LSt neurons are sexually dimorphic

Since a population of galaninergic neurons matching the LSt are present in mice already at P4, we examined whether they were sexually dimorphic in number. Our approach was to fix, clear and image in 3D the entire lumbar enlargement of pairs of male and female siblings from 5 litters. Fluorescent neurons belonging to the parallel columns running dorsolaterally of the central canal were visible in the cleared tissue and well separated in space from other zones of fluorescent puncta, including more ventrally located motoneurons (Figure 6). This allowed us, in the range L1–L5, to restrict automatic neuron counting to the volume occupied by these columns. Data from T12–T13 and L6 were excluded from analysis due to a combination of a small number of LSt neurons and greater uncertainty in their separation from more ventral and dorsal puncta.

In each of 7 sibling pairs examined, the male had more LSt neurons in L1–L5 than the female (Figure 7a). Overall, in males these neurons were significantly more numerous than in females ($p = 0.008$ pdW test) with a lower bound in the $CI_{95\%}$ of male/female ratios of 1.129 (*one sample Hodges-Lehmann estimator*; Table 1). Within our sample size the same directional difference was

detected in individual segments L2, L4, L5 ($p < 0.05$ pdW test) and L3 ($p < 0.01$ pdW test) (Figure 7a; Table 1).

3.3 | Sexual dimorphism in galanin expression is not a general phenomenon

Having established that LSt neurons are sexually dimorphic in number, we examined whether this is population-specific or the consequence of a generally higher expression level of galanin in the postnatal male mouse nervous system. Specifically, we quantified the number of fluorescent neurons in the L4 DRGs because in rodents the corresponding dermatome does not include the genitalia, being instead confined to the hindlimbs and lower back (Takahashi et al., 2003). Therefore, we did not expect *a priori* differences in primary sensory neuron numbers between sexes, in contrast to neighboring segments (e.g. L6: McKenna & Nadelhaft, 1986).

L4 DRGs from male and female siblings (n = 49) from 6 litters were fixed, cleared and imaged in 3D (Figure 4). Fluorescent neurons were counted automatically and their average number for males and females computed for each litter.

Within the power reached with our sample size we could not detect a significantly greater number of neurons in males than females ($p = 0.922$ pdW test) (Figure 7b; Table 1). We then compared the male/female ratios of LSt (n=7) and L4 DRG neurons (n=6, litter averages) and found the former to be significantly higher than the latter ($p < 0.001$ idMW test) (Figure 7c; Table 1). Furthermore, the lower bound in the $CI_{95\%}$ of the difference in such ratios was 0.149 (*two samples difference Hodges-Lehmann estimator*; Table 2). Therefore, the marked sexual dimorphism displayed by galaninergic LSt neurons at P4 is not a general phenomenon.

4 | DISCUSSION

4.1 | LSt neuron numbers and sexual dimorphism

Initial immunohistochemical investigations of galanin expression in the nervous system found neurons located in the rat lumbar spinal cord near the central canal (Ch'ng et al., 1985; Melander et al., 1986). Ju and colleagues (1987) characterized these as a well-defined population co-expressing

galanin and CCK, as well as having thalamic projections. The latter finding led to the current use of the acronym 'LSt' (lumbar spino-thalamic) when referring to this specific group, even if, to the best of our knowledge, evidence that all member neurons project to the thalamus is still missing (as acknowledged by Nicholas et al., 1999). Homologous populations of galaninergic neurons were also found in the cat (Arvidsson et al., 1991) and, recently, in humans (Chéhensse et al., 2016). LSt neurons are now thought to be a key component of a *spinal generator of ejaculation* (SGE) (Clement & Giuliano, 2016; Veening & Coolen, 2014), which makes them an important target of investigation.

Here we used a transgenic mouse line, in which the galanin promoter drives eGFP expression, to assess the early postnatal state of the LSt population. Prior studies examined adult or peri-pubertal preparations. We found brightly fluorescent neurons in a location fully consistent with their being the LSt, both with respect to segmental distribution and position relative to the central canal.

First, the number of clearly detectable galaninergic LSt neurons in the P4 male mouse (~900 L1–L5; Figure 7, Table 1) is not far from that reported for the adult male rat (~300 L1–L5: Ju et al., 1987; ~600 L1–L5: Newton, 1992b; ~471 L3–L5: Newton & Phan, 2006) and man (~500 L1–L5: Chéhensse et al., 2016). Thus, it appears that programmed cell death in the LSt population is either at an advanced stage or complete at P4, consistently with the time course observed in other thoracolumbar interneurons (Prasad et al., 2008).

Second, sexual dimorphism in LSt neuron numbers is already present at P4 (Figure 6 and Figure 7, Tables 1 and 2), much before the third postnatal week that was previously suggested for its appearance (Phelan & Newton, 2000). It is also much before the age examined by Katayama et al. (2016), who quantified GRP expression and reported sexual dimorphism at P16 in the rat. What could be the cause of sexual dimorphism at P4? A role is likely to be played by the transient perinatal androgen surge occurring in males (Oti et al., 2016). In any case, what we observed should be the organizational and not activational effects of sex hormones (Poling & Kauffman, 2013), since by P4 testosterone levels in male mice have fallen back to those of females (Clarkson & Herbison, 2016). This latter aspect might be the reason for a somewhat lower degree of dimorphism at P4 compared to estimates in adults (when testosterone levels are again higher in males).

4.2 | Possible implications of the cervical population of galaninergic neurons

While the main goal of this study was to assess the early postnatal state of LSt neurons, we deemed it important to examine the broader context of galanin expression in the spinal cord. To avoid generalizing from single cases and to account for variability among preparations, we used a quantitative approach and averaged data from several animals and litters. Galanin expression was largely consistent with prior work (see 4.3). However, we were initially surprised to find a population of neurons in the cervical and rostral thoracic segments showing a strikingly similar distribution to that of the LSt (Figure 1 and Figure 2). Careful examination of early immunohistochemical reports on galanin revealed references to this population in the adult rat (Melander et al., 1986) and cat (Arvidsson et al., 1991). Subsequent work, starting with Ju and colleagues (1987), focused on the lumbar group and its role in the control of ejaculation, and we could find no further mention of the cervical group. Given the absence of further information, one distinct possibility is that the two groups belong to the same broader neuronal population. In fact, in our data the bilateral cervical and lumbar columns appeared to be joined by sparse scattered neurons in thoracic segments, suggesting a continuum (Figure 1 and Figure 2). This raises the possibility that the neurons specifically involved in ejaculation are only a subset of the lumbar LSt group, which, in turn, could be part of a broader spinal system processing nociceptive and visceral input (Newton & Phan, 2006). It will be important in future work to examine whether this cervical population is also sexually dimorphic.

4.3 | Other sites of galanin expression in the spinal cord

A prominent feature in all segments was the intense fluorescence of the dorsal-most cord. This was in line with extensive data showing galanin expression in dorsal laminae, a major contributor being unmyelinated primary sensory afferents (Ch'ng et al., 1985). Not surprisingly, this peptide is involved in pain modulation (Xu et al., 2008). We also found many fluorescent DRG neurons (Figure 4), a result consistent with the notion that galanin accumulation in pseudo-unipolar neuron somas reaches a peak after birth (Marti et al., 1987) then decreasing to low levels in the adult (Xu et al., 1996). Interestingly, galanin expression in the ganglia can be markedly upregulated after injury

(Xu et al., 2008), a phenomenon also occurring in the autonomic nervous system (Weyne et al., 2014).

Very small galaninergic neurons were previously reported in the dorsal laminae of the newborn and adult rat (Marti et al., 1987; Melander et al., 1986). Here we could not identify them unambiguously, possibly because of the overwhelming signal coming from surrounding fibers (Ch'ng et al., 1985).

We observed fluorescence both in ventral horn cells and in ventral root fibers along the entire length of the cord (Figure 3) indicating galanin expression by motoneurons. Galanin is seldom expressed in adult motoneurons (Ch'ng et al., 1985), but a transient expression occurs in fetal and early postnatal life (Marti et al., 1987) fully consistent with our data.

One last area where we found many brightly fluorescent cell bodies was in the intermediate lateral sacral spinal cord (Figure 1 and Figure 2). This region may coincide with the spinal parasympathetic nucleus (SPN), where small galaninergic neurons were found in the adult rat (Newton, 1992a).

In summary, the distribution of galanin-expressing *neuronal cell bodies* that we found in the mouse spinal cord at P4 is consistent with previous immunohistochemistry in the adult rat or with known developmental changes occurring early in postnatal life. Our data further validates this specific mouse line as having a reporter expression corresponding to that of endogenous galanin (The GENSAT Project; Laque et al., 2013). However, one notable aspect of our data was the scarcity of fluorescent fibers and processes among LSt neurons, as well as in the thoracolumbar sympathetic and lumbosacral parasympathetic nuclei. This is at variance with the prominent galanin immunoreactivity observed in dense fiber plexa in these same regions in adult rats (Ch'ng et al., 1985; Melander et al., 1986; Newton, 1992a, 1992b). It is unlikely that this could be due to limitations in our imaging techniques, since the brightest signal in our preparations came from the fiber network located in the dorsal laminae. Instead, this may be explained by a combination of: (*i*) differences in the intracellular distribution of galanin peptide and eGFP protein; (*ii*) incomplete development of galaninergic axons at P4. In fact, given the marked developmental changes in galanin expression by sensory and motor neurons (see above), it will be important to examine

whether the lumbar (LSt) and cervical groups also modify their expression levels of this peptide postnatally.

4.4 | Conclusions

We found that galaninergic LSt neurons, thought to be strictly required for ejaculation, are present with numbers close to the adult in the early postnatal mouse. Furthermore, sexual dimorphism in their numerosity is already established at P4. These data suggest that the SGE may be sufficiently mature in the neonatal rodent spinal cord to allow functional *ex vivo* investigation, similar to what has occurred for the locomotor network (Kjaerulff & Kiehn, 1996). Furthermore, our re-discovery in cervical segments of a group of neurons similar to the LSt raises the possibility that only a subset of the lumbar population participate in ejaculation. Future studies will need to assess whether the LSt are, morphologically and functionally, a heterogeneous population.

REFERENCES

Arganda-Carreras, I., Kaynig, V., Rueden, C., Eliceiri, K. W., Schindelin, J., Cardona, A., & Seung, H. S. (2017). Trainable Weka Segmentation: a machine learning tool for microscopy pixel classification. *Bioinformatics, 33*, 2424–2426. https://doi.org/10.1093/bioinformatics/btx180

Arvidsson, U., Ulfhake, B., Cullheim, S., Bergstrand, A., Theodorson, E., & Hökfelt, T. (1991). Distribution of 125I-galanin binding sites, immunoreactive galanin, and its coexistence with 5-hydroxytryptamine in the cat spinal cord: biochemical, histochemical, and experimental studies at the light and electron microscopic level. *Journal of Comparative Neurology, 308*, 115–138. https://doi.org/10.1002/cne.903080111

Borgdorff, A. J., Bernabé, J., Denys, P., Alexandre, L., & Giuliano, F. (2008). Ejaculation elicited by microstimulation of lumbar spinothalamic neurons. *European Urology, 54*, 449–456. https://doi.org/10.1016/j.eururo.2008.03.043

Breedlove, S. M., & Arnold, A. P. (1983). Hormonal control of a developing neuromuscular system. *Journal of Neuroscience, 3*, 424–432. https://doi.org/10.1523/JNEUROSCI.03-02-00417.1983

Chapelle, P. A., Roby-Brami, A., Yakovleff, A., & Bussel, B. (1988). Neurological correlations of ejaculation and testicular size in men with a complete spinal cord section. *Journal of Neurology Neurosurgery & Psychiatry, 51*, 197–202. https://doi.org/10.1136/jnnp.51.2.197

Chéhensse, C., Facchinetti, P., Bahrami, S., Andrey, P., Soler, J. M., Chrétien, F., Bernabé, J., Clément, P., Denys, P., & Giuliano, F. (2016). Human spinal ejaculation generator. *Annals of Neurology, 81*: 35–45 https://doi.org/10.1002/ana.24819

Ch'ng, J. L., Christofides, N. D., Anand, P., Gibson, S. J., Allen, Y. S., Su, H. C., Tatemoto, K., Morrison, J. F., Polak, J. M., & Bloom, S. R. (1985). Distribution of galanin immunoreactivity in the central nervous system and the responses of galanin-containing neuronal pathways to injury. *Neuroscience, 16*, 343–354. https://doi.org/10.1016/0306-4522(85)90007-7

Clarkson, J., & Herbison, A. E. (2016). Hypothalamic control of the male neonatal testosterone surge. *Philosophical Transactions of the Royal Society B, 371*, 20150115. https://doi.org/10.1098/rstb.2015.0115

Clement, P., & Giuliano, F. (2016). Physiology and pharmacology of ejaculation. *Basic and Clinical Pharmacology & Toxicology, 119*, 18–25. https://doi.org/10.1111/bcpt.12546

Coolen, L. M., Veening, J. G., Wells, A. B., & Shipley, M. T. (2003). Afferent connections of the parvocellular suparafascicularis thalamic nucleus in the rat: evidence for functional subdivisions. *Journal of Comparative Neurology, 463*, 132–156. https://doi.org/10.1002/cne.10739

Edelstein, A., Amodaj, N., Hoover, K., Vale, R., & Stuurman, N. (2010). Computer control of microscopes using μManager. *Current Protocols in Molecular Biology, 92*, 14.20.1–14.20.17. https://doi.org/10.1002/0471142727.mb1420s92

Forger, N. (2009). The organizational hypothesis and final common pathways: sexual differentiation of the spinal cord and peripheral nervous system. *Hormones and Behavior, 55*, 605–610. https://doi.org/10.1016/j.yhbeh.2009.03.008

Forster, B., Van De Ville, D., Berent, J., Sage, D., & Unser, M. (2004). Complex wavelets for extended depth-of-field: a new method for the fusion of multichannel microscopy images. *Microscopy Research & Technique, 65*, 33–42. https://doi.org/10.1002/jemt.20092

Garcia, H. G., Lee, H. J., Boedicker, J. Q., Phillips, R. (2011). Comparison and calibration of different reporters for quantitative analysis of gene expression. *Biophysical Journal, 101*, 535–544. https://doi.org/10.1016/j.bpj.2011.06.026

Herbert, A. D., Carr, A. M., & Hoffmann, E. (2014). FindFoci: a focus detection algorithm with automated parameter training that closely matches human assignments, reduces human inconsistencies and increases speed of analysis. *PLoS ONE, 9*, e114749. https://doi.org/10.1371/journal.pone.0114749

Hershberger, S. L. (2011). Hodges-Lehmann estimators. In L. Miodrag (Ed.), *International Encyclopedia of Statistical Science* (pp.635–636). Berlin Heidelberg: Springer-Verlag. https://doi.org/10.1007/978-3-642-04898-2

Hou, B., Zhang, D., Zhao, S., Wei, M., Yang, Z., Wang, S., Wang, J., Zhang, X., Liu, B., Fan, L., Li, Y., Qiu, Z., Zhang, C., & Jiang, T. (2015). Scalable and DiI-compatible optical clearance of the mammalian brain. *Frontiers in Neuroanatomy, 9*, 19. https://doi.org/10.3389/fnana.2015.00019

Hörl, D., Rusak, F. R., Preusser, F., Tillberg, P., Randel, N., Chhetri, R. K., Cardona, A., Keller, P. J., Harz, H., Leonhardt, H., Treier, M., & Preibisch, S. (2018). BigStitcher: reconstructing high-resolution image datasets of cleared and expanded samples. *bioRxiv, 343954*. https://doi.org/10.1101/343954

Ju, G., Melander, T., Ceccatelli, S., Hökfelt, T., & Frey, P. (1987). Immunohistochemical evidence for a spinothalamic pathway co-containing cholecystokinin- and galanin-like immunoreactivities in the rat. *Neuroscience, 20*, 439–456. https://doi.org/10.1016/0306-4522(87)90103-5

Katayama, N., Oti, T., Takanami, K., Sakamoto, T., & Sakamoto, H. (2016). Postnatal development of the gastrin-releasing peptide system in the lumbosacral spinal cord controlling male reproductive function in rats. *Proceedings of the Japan Academy, Series B, 92*, 69–75. https://doi.org/10.2183/pjab.92.69

Kjaerulff, O., & Kiehn, O. (1996). Distribution of networks generating and coordinating locomotor activity in the neonatal rat spinal cord in vitro: a lesion study. *Journal of Neuroscience, 16*, 5777–5794. https://doi.org/10.1523/JNEUROSCI.16-18-05777.1996

Kirshner, H., Aguet, F., Sage, D., & Unser, M. (2013). 3-D PSF fitting for fluorescence microscopy: implementation and localization application. *Journal of Microscopy, 249*, 13–25. https://doi.org/10.1111/j.1365-2818.2012.03675.x

Kozyrev, N., Lehman, M. N., & Coolen, L. M. (2012). Activation of gastrin-releasing peptide receptors in the lumbosacral spinal cord is required for ejaculation in male rats. *Journal of Sexual Medicine, 9*, 1303–1318. https://doi.org/10.1111/j.1743-6109.2012.02688.x

Laque, A., Zhang, Y., Gettys, S., Nguyen, T.-A., Bui, K., Morrison, C. D., & Münzberg, H. (2012). Leptin receptor neurons in the mouse hypothalamus are colocalized with the neuropeptide galanin and mediate anorexigenic leptin action. *American Journal of Physiology - Endocrinology and Metabolism, **304***, E999-1011. https://doi.org/10.1152/ajpendo.00643.2012

Marti, E., Gibson, S. J., Polak, J. M., Facer, P., Springall, D. R., Van Aswegen, G., Aitchison, M., & Koltzenburg, M. (1987). Ontogeny of peptide- and amine-containing neurones in motor, sensory, and autonomic regions of rat and human spinal cord, dorsal root ganglia, and rat skin. *Journal of Comparative Neurology, 266*, 332–359. https://doi.org/10.1002/cne.902660304

McKenna, K., & Nadelhaft, I. (1986). The organization of the pudendal nerve in the male and female rat. *Journal of Comparative Neurology, 248*, 532–549. https://doi.org/10.1002/cne.902480406

Melander, T., Hökfelt, T., & Rökaeus, A. (1986). Distribution of galaninlike immunoreactivity in the rat central nervous system. *Journal of Comparative Neurology, 248*, 475–517. https://doi.org/10.1002/cne.902480404

Newton, B. W. (1992a). Galanin-like immunoreactivity in autonomic regions of the rat lumbosacral spinal cord is sexually dimorphic and varies with the estrous cycle. *Brain Research, 589*, 69–83. https://doi.org/10.1016/0006-8993(92)91163-9

Newton, B. W. (1992b). A sexually dimorphic population of galanin-like neurons in the rat lumbar spinal cord: functional implications. *Neroscience Letters, 137*, 119–122. https://doi.org/10.1016/0304-3940(92)90312-U

Newton, B. W., & Phan, D. C. (2006). Androgens regulate the sexually dimorphic production of co-contained galanin and cholecystokinin in lumbar laminae VII and X neurons. *Brain Research, 1099*, 88–96. https://doi.org/10.1016/j.brainres.2006.04.106

Nicholas, A. P., Zhang, X., & Hökfelt, T. (1999). An immunohistochemical investigation of the opioid cell column in lamina X of the male rat lumbosacral spinal cord. *Neuroscience Letters, 270*, 9–12. https://doi.org/10.1016/S0304-3940(99)00446-2

Northrup, T. [Tony & Chelsea Northrup] (2018, January 22). *Super resolution: get more megapixels!* [Video file]. Retrieved from https://youtu.be/c17MCm4lXcE

Oti, T., Takanami, K., Katayama, N., Edey, T., Satoh, K., Sakamoto, T., & Sakamoto, H. (2016). Perinatal testosterone exposure is critical for the development of the male-specific sexually dimorphic gastrin-releasing peptide system in the lumbosacral spinal cord that mediates erection and ejaculation. *Biology of Sex Differences, 7*, 1–10. https://doi.org/10.1186/s13293-016-0058-x

Phan, D. C., & Newton, B. W. (1999). Cholecystokinin-8-like immunoreactivity is sexually dimorphic in a midline population of rat lumbar neurons. *Neuroscience Letters, 276*, 165–168. https://doi.org/10.1016/S0304-3940(99)00819-8

Phelan, K. D., & Newton, B. W. (2000). Sex differences in the response of postnatal rat lumbar lamina X neurons to exogenously applied galanin recorded in vitro. *Developmental Brain Research, 122*, 157–163. https://doi.org/10.1016/S0165-3806(00)00068-7

Poling, M. C., & Kauffman, A. S. (2013). Organizational and activational effects of sex steroids on kisspeptin neuron development. *Frontiers in Neuroendocrinology, 34*, 3–17. https://doi.org/10.1016/j.yfrne.2012.06.001

Prasad, T., Wang, X., Gray, P. A., & Weiner, J. A. (2008). A differential developmental pattern of spinal interneuron apoptosis during synaptogenesis: insights from genetic analyses of the protocadherin-γ gene cluster. *Development, 135*, 4153–4164. https://doi.org/10.1242/dev.026807

Rueden, C. T., Schindelin, J., Hiner, M. C., DeZonia, B. E., Walter, A. E., Arena, E. T., & Eliceiri, K. W. (2017). ImageJ2: ImageJ for the next generation of scientific image data. *BMC Bioinformatics, 18*, 529. https://doi.org/10.1186/s12859-017-1934-z

Sage, D., Neumann, F. R., Hediger, F., Gasser, S. M., & Unser, M. (2005). Automatic tracking of individual fluorescence particles: application to the study of chromosome dynamics. *IEEE Transactions on Image Processing, 14*, 1372–1383. https://doi.org/10.1109/TIP.2005.852787

Sage, D., Donati, L., Soulez, F., Fortun, D., Schmit, G., Seitz, A., Guiet, R., Vonesch, C., & Unser, M. (2017). DeconvolutionLab2: an open-source software for deconvolution microscopy. *Methods, 115*, 28–41. https://doi.org/10.1016/j.ymeth.2016.12.015

Sakamoto, H., Matsuda, K., Zuloaga, D. G., Hongu, H., Wada, E., Wada, K., Jordan, C. L., Breedlove, S. M., & Kawata, M. (2008). Sexually dimorphic gastrin releasing peptide system in the spinal cord controls male reproductive functions. *Nature Neuroscience, 11*, 634–636. https://doi.org/10.1038/nn.2126

Schindelin, J., Arganda-Carreras, I., Frise, E., Kaynig, V., Longair, M., Pietzsch, T., Preibisch, S., Rueden, C., Saalfeld, S., Schmid, B., Tinevez, J.-Y., White, D. J., Hartenstein, V., Eliceiri, K., Tomancak, P., & Cardona, A. (2012). Fiji: an open-source platform for biological-image analysis. *Nature Methods 9*, 676–682. https://doi.org/10.1038/nmeth.2019

Schneider, J. E., Wysocki, C. J., Nyby, J., & Whitney, G. (1978). Determining the sex of neonatal mice (Mus musculus). *Behavior Research Methods & Instrumentation, 10*, 105. https://doi.org/10.3758/BF03205110

Shaefer, S., McPhail, T., & Warren, J. (2006). Image deformation using moving least squares. *ACM Transactions on Graphics, 25*, 533–540. https://doi.org/10.1145/1141911.1141920

Sun, X. Q., Xu, C., Leclerc, P., Benoît, G., Giuliano, F., & Droupy, S. (2009). Spinal neurons involved in the control of the seminal vesicles: a transsynaptic labeling study using pseudorabies virus in rats. *Neuroscience, 158*, 786–797. https://doi.org/10.1016/j.neuroscience.2008.10.008

Takahashi, Y., Chiba, T., Kurokawa, M., & Aoki, Y. (2003). Dermatomes and the central organization of dermatomes and body surface regions in the spinal cord dorsal horn in rats. *Journal of Comparative Neurology, 462*, 29–41. https://doi.org/10.1002/cne.10669

Tesson, L., Heslan, J.-M., Ménoret, S., & Anegon, I. (2002). Rapid and accurate determination of zygosity in transgenic animals by real-time quantitative PCR. *Transgenic Research* 11, 43-48. https://doi.org/10.1023/A:1013928600442

Truitt, W. A., & Coolen, L. M. (2002). Identification of a potential ejaculation generator in the spinal cord. *Science, 297*, 1566–1569. https://doi.org/10.1126/science.1073885

Truitt, W. A., Shipley, M. T., Veening, J. G., & Coolen, L. M. (2003). Activation of a subset of lumbar spinothalamic neurons after copulatory behavior in male but not female rats. *Journal of Neuroscience, 23*, 325–331. https://doi.org/10.1523/JNEUROSCI.23-01-00325.2003

The Gene Expression Nervous System Atlas (GENSAT) Project, NINDS Contracts N01NS02331 & HHSN271200723701C to The Rockefeller University (New York, NY).

Veening, J. G., & Coolen, L. M. (2014). Neural mechanisms of sexual behavior in the male rat: emphasis on ejaculation-related circuits. *Pharmacology Biochemistry & Behavior, 121*, 170–183. https://doi.org/10.1016/j.pbb.2013.12.017

Weyne, E., Albersen, M., Hannan, J. L., Castiglione, F., Hedlund, P., Verbist, G., De Ridder, D., Bivalacqua, T. J., & Van der Aa, F. (2014). Increased Expression of the Neuroregenerative Peptide Galanin in the Major Pelvic Ganglion Following Cavernous Nerve Injury. *Journal of Sexual Medicine, 11*, 1685–1693. https://doi.org/10.1111/jsm.12570

Xu, Z.-Q., Shi, T.-J., & Hökfelt, T. (1996). Expression of galanin and galanin receptor in several sensory systems and bone anlage of rat embryos. *Proceedings of the National Academy of Sciences*, 93, 14901-14905. https://10.1073/pnas.93.25.14901

Xu, C., Giuliano, F., Yaici, E. D., Conrath, M., Trassard, O., Benoit, G., & Vergé, D. (2006). Identification of lumbar spinal neurons controlling simultaneously the prostate and the bulbospongiosus muscles in the rat. *Neuroscience, 138*, 561–573. https://doi.org/10.1016/j.neuroscience.2005.11.016

Xu, X.-J., Hökfelt, T., & Wiesenfeld-Hallin, Z. (2008). Galanin and Spinal Pain Mechanisms: Where Do We Stand in 2008? *Cellular and Molecular Life Sciences, 65*, 1813–1819. https://doi.org/10.1007/s00018-008-8155-6

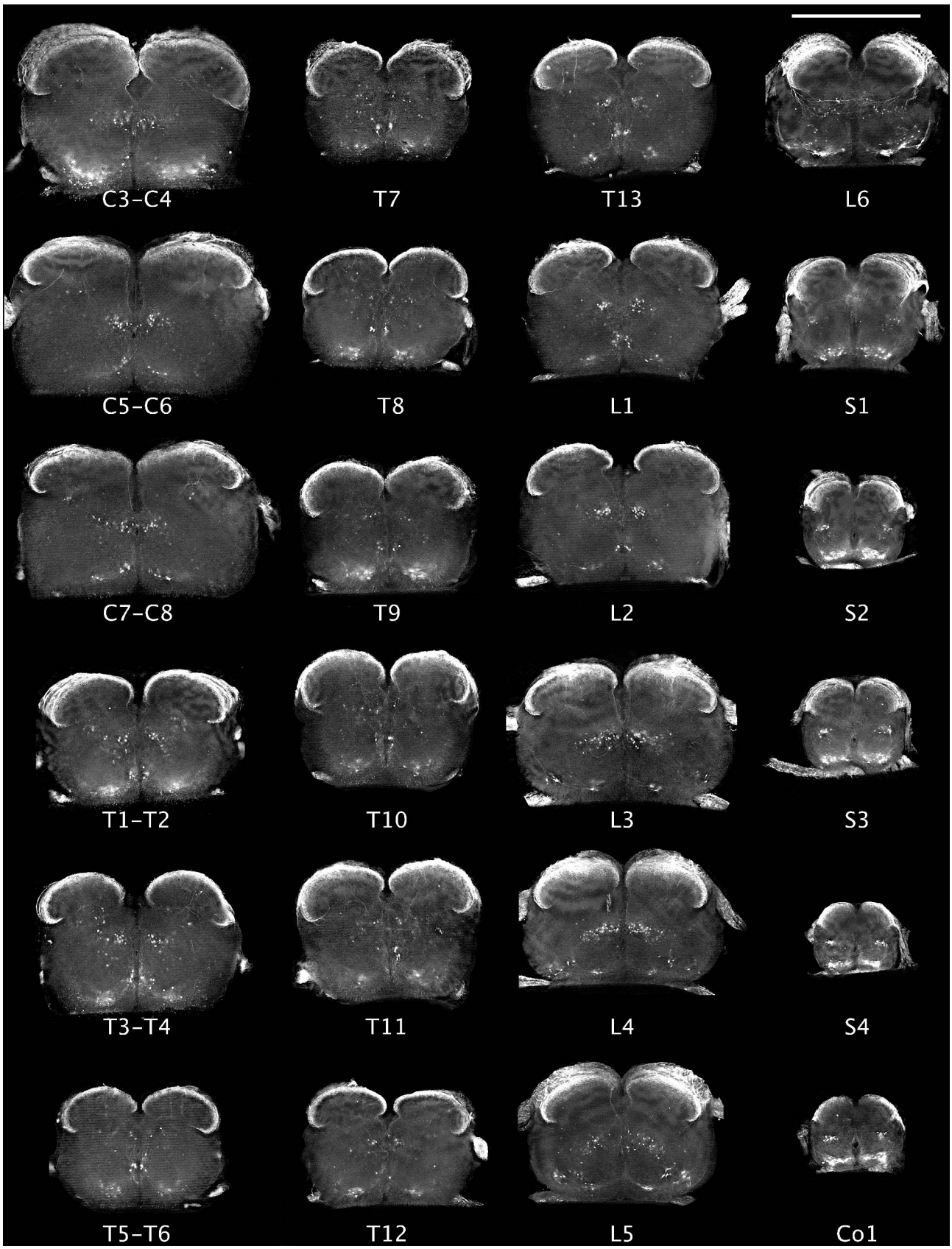

FIGURE 1 Segmental distribution of fluorescence expression in the Gal-eGFP$^{+/+}$ mouse at P4 viewed in live transverse slices. The slices are representative examples from each segment. Original stacks were acquired with a 4x air objective, deconvolved and the in-focus slice surface extracted (see 2.3 and 2.3.1). For display purposes the contrast of each slice (black and white points) was adjusted independently. Scale bar: 1000 μm.

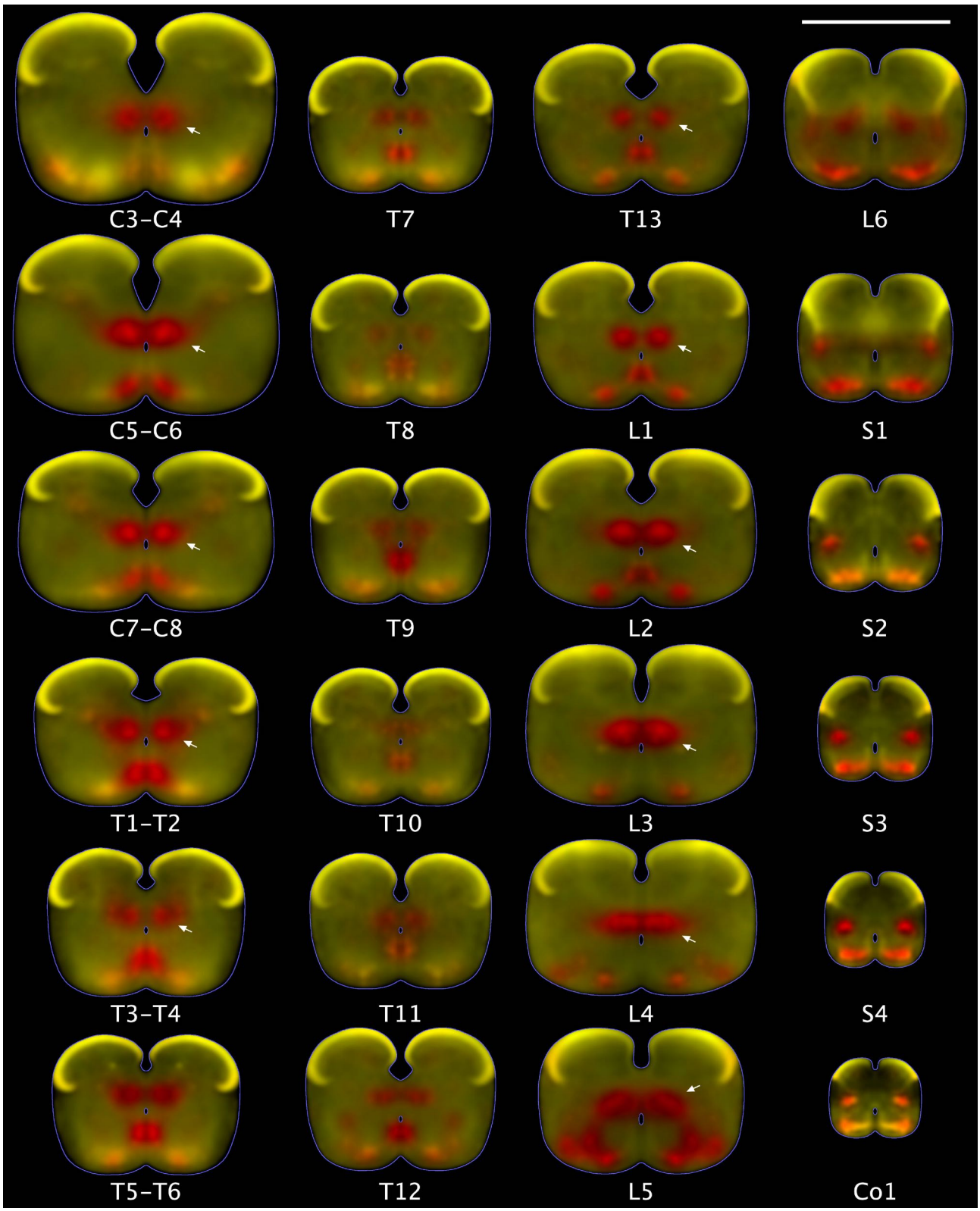

FIGURE 2 Average segmental distribution of fluorescent fibers (yellow) and neuronal somas (red) in the Gal-eGFP$^{+/+}$ mouse at P4. Images were obtained by averaging slices, in register, from several animals both females and males, log-transforming and normalizing fluorescence intensity. Color coding was processed separately by training a pattern recognition algorithm to identify fluorescent cell bodies; thus, areas of fluorescent fibers (or other unidentified sources) were colored yellow, while identified neuronal somas were colored red (see 2.3.1). White arrows point to a lumbar group of fluorescent neurons, likely corresponding the the lumbar spino-thalamic (LSt) thought to be involved in

ejaculation, and an unexpected cervical population having a similar spatial distribution. Dorsal is up. Scale bar: 1000 μm.

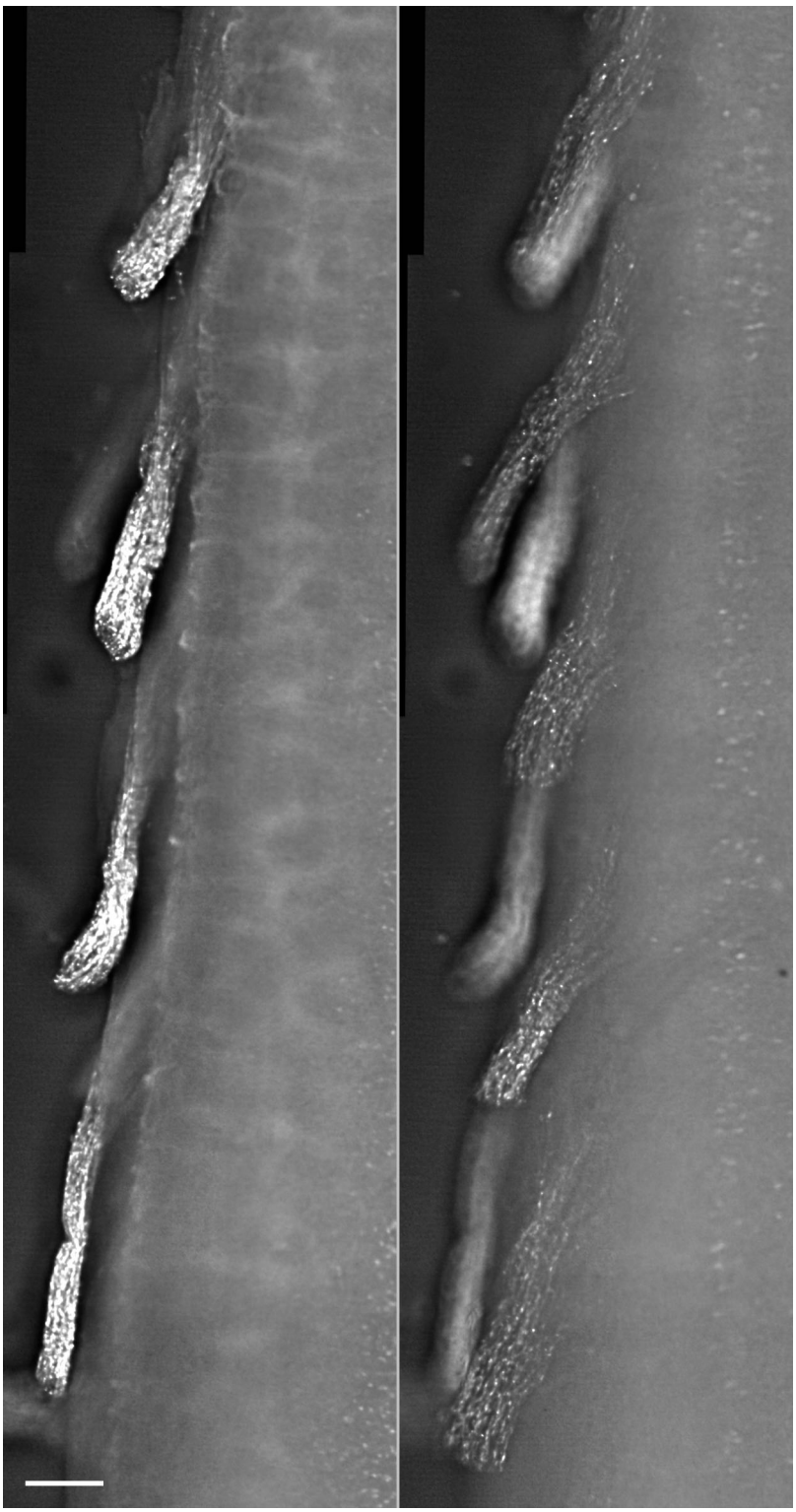

FIGURE 3 View of a rostral lumbar enlargement in a fixed and cleared spinal cord from a P4 mouse, showing brighter fluorescence in dorsal than in ventral roots. (left) The T12–L2 dorsal roots are in focus. (right) The T12–L3 ventral roots are in focus; a column of dimly fluorescent presumed motoneurons is also visible. The same acquisition parameters, processing and contrast were used for the two panels. The preparation was viewed from the ventral side and the original stacks were acquired with a 4x air objective, deconvolved and stitched in a single composite. Rostral is up. Scale bar: 200 μm.

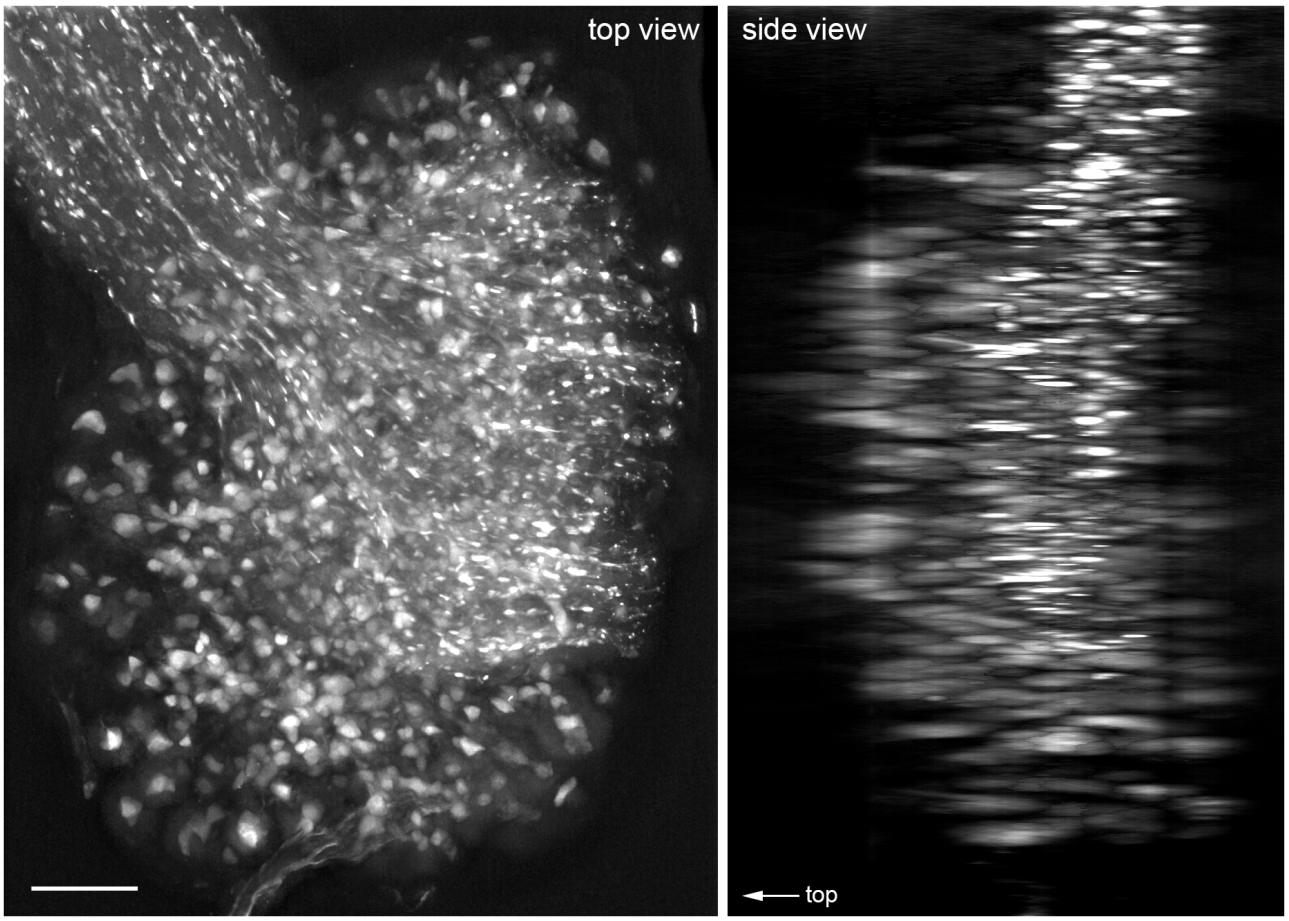

FIGURE 4 Example of fixed and cleared L4 DRG from a female mouse at P4 showing a large number of fluorescent primary sensory neuron somas and axons. (left) Max intensity projection along the z-axis giving a top view of the DRG (i.e. from the direction of the objective). Dorsal root fibers containing small brightly fluorescent puncta are visible as they emerge from the ganglion. (right) max intensity projection along the x-axis giving a side view of the DRG. A single stack was acquired with a 10x water objective and deconvolved. Scale bar: 100 μm.

FIGURE 5 Dorsal view reconstruction of live spinal cords from female (left, rostral at the top) and male (right, rostral at the bottom) siblings at P4, arranged side-by-side in a head to tail fashion. A web-like network of fluorescent fiber bundles is visible on the dorsal surface of the Gal-eGFP$^{+/+}$ mouse. This fluorescence source must contribute to the overall fluorescence emitted by the dorsal-most spinal cord when viewed in transverse slices (Figure 1 and Figure 2). The composite was obtained by stitching together 19 images acquired with a 4x air objective, each obtained by deconvolution and 'extended depth of field' of the acquired stack. Scale bar: 1000 μm.

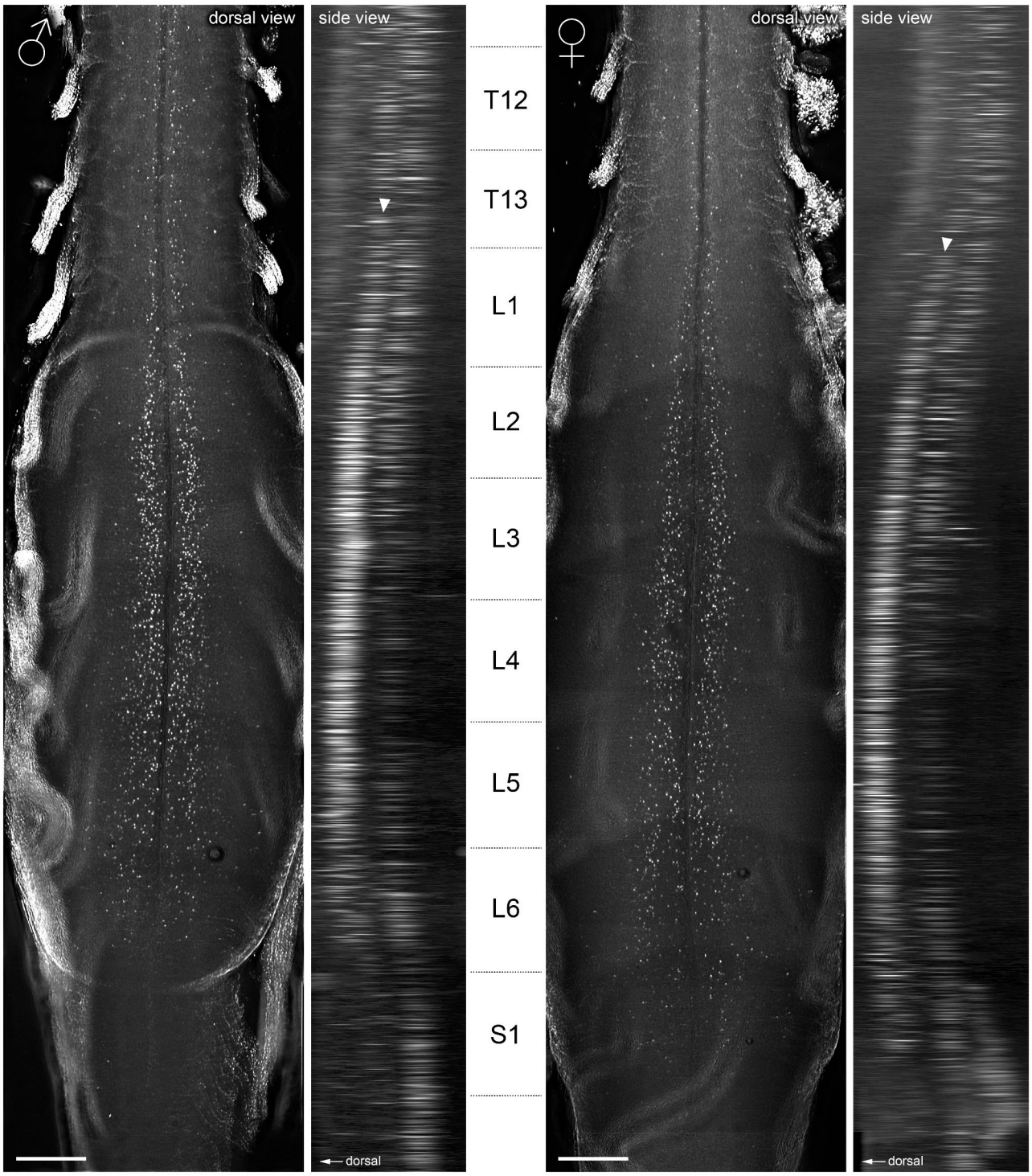

FIGURE 6 Fixed and cleared lumbar enlargements from male (left) and female (right) siblings at P4 showing a greater number of lumbar spino-thalamic (LSt) neurons in the male. (dorsal view panels) Max intensity projections along the z axis, restricted to the volume containing LSt neurons. (side view panels) Max intensity projections along the x-axis restricted to the medial cord. White arrows point to the location of the LSt neuron band; the separate band immediately to its right is most probably composed of motoneurons. In the side views individual neurons appear as long streaks due to the well-known lower axial (z-axis) resolution of optical systems. The same acquisition parameters, processing, display contrast and gamma were used for the two preparations. Original stacks were acquired with a 4x air objective, deconvolved, stitched in a single composite and LoG 3D filtered to enhance ellipsoidal particles on the neuronal scale. Scale bar 500μm for all panels.

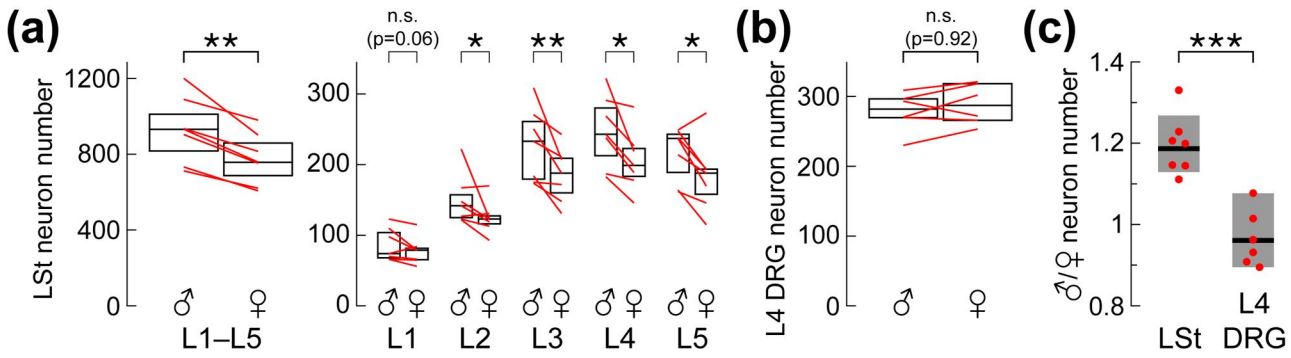

FIGURE 7 Descriptive and inferential statistics of galanin-expressing LSt and L4 DRG neuron counts in males and females. (a) The number of fluorescent LSt neurons in the lumbar enlargement (L1–L5) and in individual segments. In males their number was significantly higher. (b) The number of fluorescent neurons in the L4 DRG. No evidence was found of their number being higher in males. (c) Male/female ratios in the number of galanin-expressing LSt neurons (L1–L5) and L4 DRG neurons. The LSt neuron ratios were significantly higher than those of L4 DRG ones. Box plots in A and B show medians and interquartile ranges. Black lines and gray boxes in C show Hodges-Lehmann estimators and their $CI_{95\%}$. Red lines and dots show the underlying data. * $p < 0.05$, ** $p<0.01$, *** $p<0.001$.

TABLE 1 Descriptive and inferential statistics of galaninergic LSt and L4 DRG neuron counts in males and females

	litters	samples		median		H-L		$CI_{95\%}$ H-L		p (♂>♀) pdW test	♂/♀ H-L	♂/♀ $CI_{95\%}$ H-L
		♂	♀	♂	♀	♂	♀	♂	♀			
LSt: L1–L5	5	7	7	931	758	**925**	**773**	732-1089	621-902	**0.008**	**1.187**	**1.129-1.268**
LSt: L1	5	7	7	74	79	86	75	68-110	61-100	0.064		
LSt: L2	5	7	7	142	123	145	123	123-185	106-147	0.039		
LSt: L3	5	7	7	233	188	225	188	175-280	148-225	0.008		
LSt: L4	5	7	7	243	199	248	203	187-296	168-251	0.011		
LSt: L5	5	7	7	237	188	220	182	164-248	143-233	0.023		
DRG: L4	6	6 (23)	6 (26)	282	287	282	287	230-309	253-321	**0.922**	**0.961**	**0.895-1.077**

Key data are set in bold. Neuron number parameters are rounded to the nearest integer. Samples for L4 DRGs are given as: intra-litter averages (raw number of ganglia). H–L: Hodges-Lehmann estimator of the center of a distribution.

TABLE 2 Inferential statistics on sexual dimorphism comparing galaninergic LSt versus L4 DRG neurons

	♂/♀ H-L		♂/♀ $CI_{95\%}$ H-L		p (♂/♀LSt > ♂/♀DRG) idMW test	♂/♀LSt – ♂/♀DRG H-L	♂/♀LSt – ♂/♀DRG $CI_{95\%}$ H-L
	LSt: L1–L5	DRG: L4	LSt: L1–L5	DRG: L4			
sexual dimorphism	1.187	0.961	1.129-1.268	0.895-1.077	**<0.001**	0.237	**0.149-infinity**

Key data are set in bold. H-L: Hodges-Lehmann estimator of the center (columns 2–5) or the difference in centers (last two columns) of a distribution.